doi:10.1016/j.ultrasmedbio.2010.05.011

● *Original Contribution*

A STUDY OF BUBBLE ACTIVITY GENERATED IN *EX VIVO* TISSUE BY HIGH INTENSITY FOCUSED ULTRASOUND

JAMES MCLAUGHLAN,* IAN RIVENS,* TIMOTHY LEIGHTON,[†] and GAIL TER HAAR*

*The Institute of Cancer Research, Joint Department of Physics, Royal Marsden NHS trust, Sutton, Surrey, UK; and [†] Institute of Sound and Vibration Research, Southampton University, Highfield, Southampton, UK

Abstract—Cancer treatment by extracorporeal high-intensity focused ultrasound (HIFU) is constrained by the time required to ablate clinically relevant tumour volumes. Although cavitation may be used to optimize HIFU treatments, its role during lesion formation is ambiguous. Clear differentiation is required between acoustic cavitation (noninertial and inertial) effects and bubble formation arising from two thermally-driven effects (the vapourization of liquid into vapour, and the exsolution of formerly dissolved permanent gas out of the liquid and into gas spaces). This study uses clinically relevant HIFU exposures in degassed water and *ex vivo* bovine liver to test a suite of cavitation detection techniques that exploit passive and active acoustics, audible emissions and the electrical drive power fluctuations. Exposure regimes for different cavitation activities (none, acoustic cavitation and, for *ex vivo* tissue only, acoustic cavitation plus thermally-driven gas space formation) were identified both in degassed water and in *ex vivo* liver using the detectable characteristic acoustic emissions. The detection system proved effective in both degassed water and tissue, but requires optimization for future clinical application. (E-mail: jmclaughlan7@gmail.com)   © 2010 World Federation for Ultrasound in Medicine & Biology.

Key Words: Active cavitation detection, Ultrasonic acoustic emissions, B-mode, Boiling, HIFU, Passive cavitation detection, Drive power fluctuations, Audible emissions.

INTRODUCTION

High-intensity focused ultrasound (HIFU) can be used for noninvasive thermal ablation of soft tissue tumours deep within the body (Kennedy 2005). The volume of tissue damage created by a single HIFU exposure (referred to as a *lesion*) is small compared with that of the tumours being targeted. This results in long treatment times (ter Haar 1995) and is a factor deterring HIFU treatments from becoming more widely implemented clinically. Although it is thought that cavitation can be used to optimize HIFU treatments (Coussios et al. 2007), there is some ambiguity as to its role during lesion formation.

Negative acoustic pressures (~1 to 5 MPa) generated during the rarefaction portion of the HIFU pressure cycle cause tension in the tissue that can lead to the formation and/or activity of gas or vapour-filled cavities, known as *acoustic cavitation* (Neppiras 1980, 1984). Acoustic cavitation has been categorized into two types: noninertial (stable) and inertial (transient or collapse). However, cavitation can also be generated by the thermally-driven formation of gas spaces as a result of the high temperatures caused by HIFU exposures. It is conventional to use the word ''boiling'' to describe this nonacoustic, thermal mechanism of bubble formation during HIFU. However, it is important to note that such thermally-mediated gas pocket formation involves exsolution of the permanent gas phase as well as vapourization of water, and some degree of both exsolution and vapourization can occur at temperatures below that required to reach the boiling point (*i.e.*, when the vapour pressure in the liquid equals the static pressure). Compliance with the conventional use of the phrase ''boiling cavitation'' in this paper is therefore undertaken with the qualification that the phrase refers to thermally-mediated gas pocket formation during HIFU and not necessarily to reaching the boiling point in tissue.

The focal volumes of HIFU beams (at 1.69 MHz) are typically ellipsoidal, 1–2 mm in diameter and 15–20 mm in length (Watkin et al. 1996) and are thus significantly larger than the volume occupied by individual acoustic

Address correspondence to: Dr. James McLaughlan, Royal Marsden NHS Trust, The Institute of Cancer Research, Joint Department of Physics, Room 317, 110 Cummington Street, Boston, MA 02215. E-mail: jmclaughlan7@gmail.com

cavitation ($\sim \mu$m) and boiling bubbles ($\sim$mm). Both types of bubble activity may occur within the focal region during the exposure of absorbing media.

There are a number of acoustic cavitation detection techniques (Leighton et al. 1996; Bailey et al. 2003; ANSI 2002; Leighton et al. 2005; Coussios et al. 2007). The one most commonly used with ultrasound exposures is passive cavitation detection (PCD) of the acoustic emissions generated by bubbles (Hynynen 1991; Coleman et al. 1992; Everbach et al. 1997; Poliachik et al. 1999; Zeqiri et al. 2003; Tu et al. 2006; Chitnis et al. 2006; Hwang et al. 2006), and indeed in some circumstances automated real-time judgements based on PCDs have outperformed radiologist judgements (Leighton et al. 2008). The sensors used for PCD are usually focused to maximize signal sensitivity and spatial specificity. The acoustic frequencies emitted are determined by the bubble behavior and the amplitude and frequency (f_0) of the HIFU drive. Both noninertial and inertial acoustic cavitation events have been shown to generate emissions at subharmonics (f_0/n_i) and superharmonics ($n_i f_0$) of the drive frequency, although it is believed that the violent collapse of inertial cavitation bubbles is the only source of broadband emissions (Chen et al. 2003). Superharmonic emissions are rarely used as indicators of acoustic cavitation because they are also generated by nonlinear propagation in HIFU fields (Meaney et al. 2000; Filonenko and Khokhlova 2001; Leighton 2007), making it difficult to differentiate between signals arising from these two sources. The availability of such a wide range of detectable signals, plus the requirement for rapid sampling (relative to the ultrasound frequency), generates such sizeable datasets that processing the output presents challenges. As a result, much of the existing literature is anecdotal, with typical or example datasets being shown, thus avoiding the advantages of data averaging from repeated experiments. More recently, this has begun to be addressed, *e.g.*, with the reporting of trends as a function of driving pressure in the average of a signal (*e.g.*, subharmonic or broadband; Mast et al. 2008). However there remains the question of whether presentation of a single metric, obtained during exposure, is sufficiently informative for current applications, which include attempts to optimize HIFU treatment using cavitation feedback control (Coussios et al. 2007).

Active cavitation detection (ACD) uses pulse-echo ultrasound to detect bubbles (Medwin 1977; Miller 1981; ter Haar and Daniels 1981; Roy 1990; Holland et al. 1996; Deng et al. 1996; Melodelima et al. 2004; Tu et al. 2006). Commercially available real-time diagnostic ultrasound could be used for this purpose, but radio-frequency signals from the HIFU field can interfere with B-mode imaging, meaning that it may be necessary to interrupt HIFU exposures briefly to capture images (Vaezy et al. 2001). Even in combination with PCD, it can be difficult to differentiate between areas of B-mode hyperechogenicity generated during HIFU exposure *in vivo* by acoustic bubbles from those caused by boiling bubbles (Rabkin et al. 2005, 2006). Bailey *et al.* (2001) used overpressure to elucidate the role of bubbles in distorting HIFU lesions in *ex vivo* liver. The study demonstrated that bubble formation resulted in "tadpole"-like lesion shapes. Although overpressure increases the boiling temperature and dissolution rate, and suppresses bubble oscillations, the study did not specify whether the observed hyperechogenicity associated with lesion distortion was dominated by acoustic cavitation, boiling and/or thermal exsolution. Thus, further investigation of the use of B-mode imaging for this purpose is needed.

PCD and ACD have been used to complement each other in a number of different media. There exist extensive studies of HIFU exposures in gel phantoms (Khokhlova et al. 2006) and tissue, both *ex vivo* and *in vivo* (Hynynen 1991; Sokka et al. 2003; Anand and Kaczkowski 2004; Melodelima et al. 2004; Rabkin et al. 2006; Mast et al. 2008), using passive (ultrasonic frequencies only) and/or active cavitation detection.

A less commonly used detection technique (Coakley 1971; Neppiras and Coakley 1979) monitors the electrical drive power fluctuation caused by acoustic backscatter from bubbles. Originally applied in liquids, this technique has only been used in gel phantoms with HIFU (Thomas et al. 2006). A second, more anecdotal, technique records audible acoustic emissions produced during HIFU exposures. Several authors have reported popping sounds (Illing et al. 2006; Khokhlova et al. 2006; Silverman et al. 2006), with some likening the noise to cooking popcorn (Sanghvi et al. 1995; Crum and Law 1995) and others describing a high-pitched noise attributed to inertial cavitation (Chen et al. 2003). No study has presented quantitative analysis of audible data (although audible emissions have been correlated with sonochemical and luminescent markers of inertial cavitation in aqueous solution; Birkin et al. 2003).

The cavitation detection system presented next incorporates simultaneous PCD (MHz ultrasound emissions), ACD, measurement of the drive power fluctuation and quantification of audible (1 to 20 kHz) acoustic emissions to explore the extent to which these signals reflect the presence of acoustic cavitation and boiling bubbles (McLaughlan et al. 2007a, 2007b). In an attempt to broaden the understanding of cavitation activity during HIFU, this comprehensive suite of measurement techniques is implemented simultaneously with a view to assessing the clinical potential of each technique. Data collection and signal processing techniques have been investigated in both degassed water and *ex vivo* liver

tissue to provide a robust multispectrum approach that builds on the existing knowledge reviewed here before. The overall aim of this study was to determine whether a system designed to allow continuous simultaneous investigation of complementary detection techniques from short (≤10 s) continuous HIFU exposures might be useful in optimizing clinical HIFU treatment times by exploitation, or control, of cavitation activity. The temporal behavior of the parameters studied has been recorded, with the cumulative information from repeat exposures being investigated for their potential use as a measure of clinical outcome. The next step toward clinical development will be optimization of specific measuring hardware, but this was not investigated here. No attempt has been made to determine cavitation thresholds in these preliminary studies. Instead, clearly distinguishable regimes of different cavitation activity have been chosen. This avoids the potential problem that the apparent "cavitation threshold" measured by a given technique might be most representative of the detection threshold for that sensor. The results of this study, which uses novel methods, in addition to PCD and ACD, for HIFU monitoring, will inform future threshold studies. During the review and revision of this paper, other detection systems using combinations of detection techniques have been described (see Addendum).

MATERIALS AND METHODS

HIFU drive and cavitation detection equipment

A 1.69-MHz focused bowl piezoceramic transducer (f-number 1.79, focal length 15 cm), previously used clinically (Visioli et al. 1999), was used to generate clinically relevant HIFU intensities and exposure durations in *ex vivo* bovine liver tissue. The intensity (free-field spatial-peak) was determined using a radiation force balance (Hill et al. 1994). Repeat measurements gave a spread in intensity values of $\pm10\%$ ($n = 16$). The focal beam pressure profile (6 dB radial and axial full width half maximum [FWHM] of 2.0 and 16 mm) and free-field peak-negative pressure values were measured for 80-cycle pulses using a calibrated 0-5 mm element polyvinylidene fluoride (PVDF) membrane hydrophone (GEC Marconi, Portsmouth, UK). The spread in repeat measured peak–negative pressures was $\pm7\%$ ($n = 9$). The free-field intensity and pressure were corrected (neglecting nonlinear propagation harmonics) to give *in situ* levels in *ex vivo* bovine liver using an attenuation of 0.11 Np/cm at 1.7 MHz (Duck 1990). All HIFU exposures are quoted as *in situ* spatial-peak intensities (I_{sp}), with the *in situ* focal peak–negative pressure given in brackets.

A timer (0.01-s resolution) was used to control HIFU exposure by triggering both a function generator (Agilent 33120a, Santa Clara CA, USA) and a data acquisition

system (detailed later). The function generator signal was passed to an amplifier (ENI A300, +55 dB), which was connected to the HIFU transducer via a 'pick-off' box containing a potential divider and inductor to measure voltage (V) and current (i), respectively.

The data acquisition system (DAQ) consisted of two eight-bit four-channel boards (Spectrum Inc. MI.2031 and MI.2021, Grosshansdorf, Germany) installed in a dual PCI-bus PC (Super Micro Computer Inc, San Jose CA, USA, Pentium 4, 4 GB RAM). The dual PCI-bus allowed simultaneous streaming of data from both acquisition cards directly to RAM using a first in, first out function built into the cards, controlled by a C++ program. This allowed data acquisition on four separate channels at up to 50 MHz (limited by the PCI bus speed). The four channels were used to monitor two passive detectors (detailed later) and the drive voltage and current (see next section). Although large amounts of data could be recorded over exposure periods up to 8 s ($\sim$125 MB/s), it was not possible to display the signals in real time.

The PCD part of the detection system, shown in the left schematic in Fig. 1, comprised two focused detectors (Olympus NDT Inc, Waltham, MA, USA): A 1-MHz receiver (1.5-cm diameter, focal length 4 cm, bandwidth 0.1 to 2 MHz) and a 10-MHz sensor (3.0-cm diameter, focal length 4.5 cm, bandwidth 5 to 12 MHz). The relative sizes of the 6-dB contours of the HIFU focus and the two PCD detectors foci are indicated in Fig. 1. Two filters (Allen Avionics, Mineola, NY, USA), one low-pass (F5099, 850-kHz cut off, 80-dB attenuation at 1.69 MHz, 25 dB/decade) and one high-pass filter (F5100, 6-MHz cut off, 90-dB attenuation at 1.69 MHz, 25 dB/decade) were used, as shown in Fig. 1, to avoid saturation of the detection system by radiofrequency pickup from the drive signal, and acoustic interference from the HIFU system. A 20-dB preamplifier (7866, 0.1 to 30 MHz bandwidth, Advanced Receiver Research, Burlington, CT, USA) was used with each passive transducer. This allowed simultaneous investigation of the half harmonic, superharmonics and high-frequency broadband emissions. The 1- and 10-MHz sensors were aligned with the HIFU focal peak by pulsing a 40 cycle HIFU burst from a (1-mm diameter) ball bearing target (McLaughlan et al. 2010).

The right hand schematic in Fig. 1 shows the Z.One diagnostic scanner (Zonare, Mountain View, CA, USA) with an L10.5 linear array probe (center frequency 8 MHz, 6-cm maximum imaging depth, frame rate 14 Hz) used for ACD. The scanner collected data continuously from just before, during and for up to 10 s after HIFU exposure. No gating techniques to allow interleaving of B-mode image acquisition with HIFU exposures were used, and thus images obtained during HIFU were susceptible to interference caused by detection by the imaging probe of the scattered HIFU signal. Concern
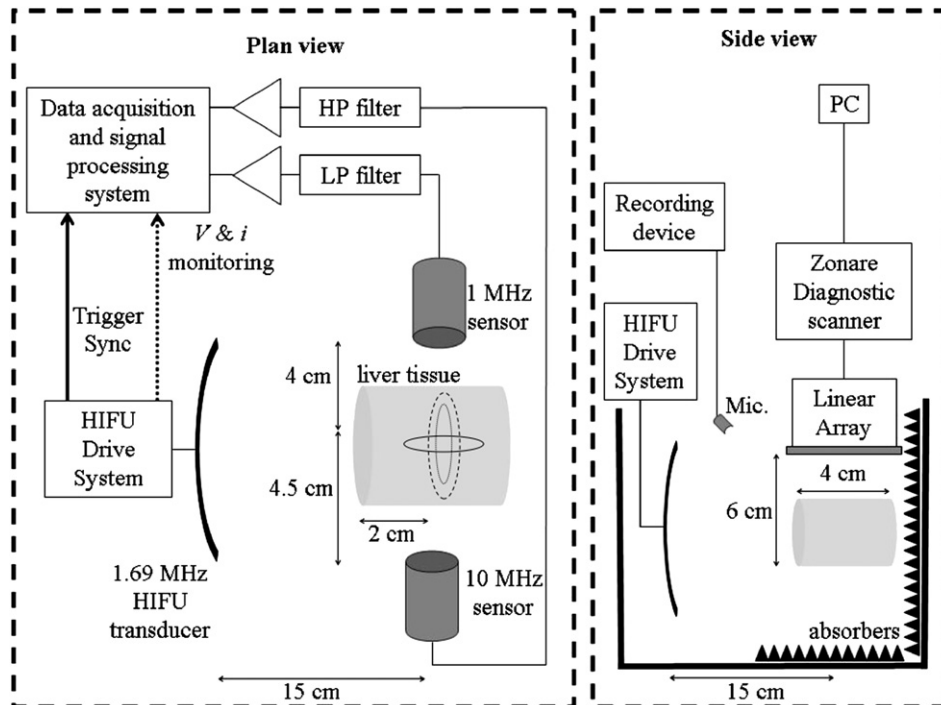
Fig. 1. Plan (left) and side view (right) of the experimental setup used for the degassed water and ex vivo tissue study. The tank is omitted from the plan view for clarity. The relative (to each other) focal sizes of the HIFU (solid line, radial FWHM 2 mm, axial FWHM 16 mm), 1 MHz (dotted line, radial FWHM 4 mm, axial FWHM 30 mm) and 10 MHz (dashed line, radial FWHM 2 mm, axial FWHM 15 mm) transducers are shown.

about the detection of scanner signals by the PCD sensors meant that ACD was not used at the lowest intensities to minimize the possibility of false-positive detection of inertial cavitation. It was therefore only used in 5/45 exposures (all of which exhibited acoustic cavitation, and three of which also resulted in boiling).

A microphone (CHK00627, frequency response 0.03 to 17 kHz, 80-dB signal/noise; Partridge Electronics, Essex, UK) connected to a PC digital recording device (16-bit resolution), and positioned as shown in Fig. 1 (*left*), was used to digitally encode audible emissions (1 to 22.4 kHz) at a rate of 44.8 kHz.

Sensor validation was undertaken in aqueous solution. After earlier demonstrations of the quantitative cross-validation of several sensors for inertial cavitation (Leighton et al. 2005), the ultraviolet spectroscopic change in potassium iodide solution was used as an indicator of inertial cavitation. Against this benchmark, the performance of the PCD in detecting broadband emissions only in the presence of inertial cavitation for this HIFU exposure system was confirmed (McLaughlan et al. 2006, 2010). In a qualitative study designed to characterize audible signals arising solely from tissue boiling, and to exclude possible contributions from acoustic cavitation, emissions were monitored from tissues heated to the boiling point using microwave energy (McLaughlan et al. 2010).

Signal processing and analysis

Voltage (V) and current (i) recorded using two channels of the DAQ (sampling rate 12.5 MHz) were used to calculate the average electrical drive power (P):

$$P = \frac{1}{N\tau} \int_0^{N\tau} V(t)i(t)dt, \qquad (1)$$

where the integration was performed in the steady state over 500 acoustic cycles (N) with period τ, resulting in a temporal resolution of 0.3 ms. The minimum sensitivity of this measurement was ± 0.125 W, determined by driving the HIFU system into a high-power 50 Ω load. Summing data over 500 cycles minimizes effects of inherent phase differences between voltage and current (caused by impedance mismatch) such that power fluctuations reflect impedance changes caused by bubble formation in the acoustic propagation path. Although reducing the data volume that can be manipulated in software, this method retains sufficient temporal information to allow comparison with the frequency spectra of the emissions data that were sampled every millisecond. Power fluctuations are also represented by the standard deviation of the averaged level for 100 sequential data points ($\sim$4 ms).

The data recorded from each passive sensor ($\sim$1 GB) were subdivided into groups of 4096 points (temporal

resolution 1 ms; spectral resolution 1.5 kHz for a sample rate of 25 MHz) and a fast Fourier transform (FFT) calculation using a Hanning window function (Smith 1997), was performed on each group. For each dataset, the peak spectral amplitudes of the half and fourth harmonic (of the HIFU drive, peak detected over ±7.5 kHz about the frequency of interest) were calculated over the entire exposure time. The fourth harmonic was selected for analysis because it was the lowest superharmonic outside the high-pass filter frequency band, and thus provided the greatest signal amplitude from an attenuating medium. However, at the higher drive settings, there is a low level of fourth harmonic emission arising from nonlinear propagation, a time at which a rapid and substantial increase in its amplitude could be identified. An ''onset time'' has therefore been defined as the first time at which the amplitude is greater by at least a factor of 10 than its nearest neighbor values during the exposure. The level of broadband emission was obtained using a two-step process. Following the FFT calculation, a ''comb'' software filter was used to remove any harmonics (produced by nonlinear propagation) and subharmonics of the drive signal from the data. This filter set the amplitude of the spectrum for a region 200 kHz wide around each $n_i f_0/2$ ($n_i = 1$ to 30) harmonic to zero, to prevent their contribution to the broadband signal. Summation of amplitudes in the resultant discontinuous frequency band gave the ''integrated broadband'' emission amplitude over the entire exposure time. Thus, half and fourth harmonic, and integrated broadband amplitudes, could be plotted as a function of time. In addition, the data up to each time point was summed to provide a cumulative measure of each quantity with the baseline noise level removed, to assess whether such information could provide a useful method for averaging the highly stochastic cavitation data sampled at high rates (25 MHz) over relatively long exposures (4 s).

For the binary analysis, an emission was said to have occurred when the signal was detected by the PCD over a minimum of five data points, each of which was at least five times greater than the exposure noise level (defined as the peak of the signal that was recorded for 0.5 s after the HIFU exposure). In addition, a baseline noise level was established from the peak of a ''sham'' exposure, for which the electrical drive system was run at the highest drive level; with the HIFU transducer disconnected, this value was derived from the data shown. Averaging these measurements over exposure time for 15 samples gives noise levels of 0.3 ± 0.15 mVrms for half harmonic, 0.2 ± 0.03 mVrms for fourth harmonic and 0.12 ± 0.07 Vrms.Hz for broadband emissions (McLaughlan et al. 2010).

After every HIFU exposure, each B-mode image frame was downloaded to a PC, and in-phase and quadrature (IQ) data were converted to radiofrequency and B-mode data using MATLAB (The MathWorks, Inc., Natick, MA, USA) routines provided by Zonare. The presence of hyperechogenicity was assessed by comparison of reference (pre-HIFU) images, with those obtained immediately post exposure. The reference frame was subtracted from the post-HIFU frame, using the image subtraction routine available in the MATLAB image processing toolbox. This process allowed identification of regions of increased echo level that were different in appearance from noise-related speckle change. Temporal frequency analysis was performed on the radiofrequency data using a MATLAB routine written in-house that identified specific frequency components in the B-mode images that could be related to the HIFU exposure.

Audible emission data were processed using a MATLAB (The MathWorks, Inc.) routine that extracted temporal information by using 2048 points per FFT calculation, yielding a temporal resolution of 50 ms. Baseline noise, caused by ambient noise levels in the laboratory (in particular the power amplifier and air conditioning unit), was measured for 1 s after each HIFU exposure. Audible emissions were positively identified during an exposure if broadband signals were detected in the 1–20 kHz range above the baseline noise level. These could also be clearly heard when the recorded data were replayed.

HIFU exposure

Unfiltered tap water was degassed by placing under a tension of 0.85 MPa for a minimum of 12 h. A dissolved oxygen meter (HQ30d with a LDO101 probe, HACH LANGE Ltd., Manchester, UK) measured gas content to be 4.5 and 5.6 ± 0.01 mg/L before and after a 5-h experiment, respectively. Degassed water was exposed to 4-s HIFU exposures at spatial-peak intensities (I_{sp}) of 550, 1100 and 2200 ± 10% W/cm^2 (peak negative pressures 1.88, 2.10 and 2.32 ± 7% MPa). For a water volume (~27,000 cm^3) significantly larger than the focal volume of the 1.69-MHz transducer (~0.3 cm^3), it was verified experimentally that repeated (>20) exposures in the degassed water did not change the I_{sp} levels required to produce detectable acoustic cavitation. This is probably because radiation force causes streaming and moves any bubbles away from the focal region between successive exposures.

The freshly excised *ex vivo* bovine liver used in this study was collected from an abattoir and stored overnight in a refrigerated room (5 to 10 °C). Individual cylindrical samples (50 mm diameter, 45 mm long) were cut, submerged in room temperature degassed water and degassed to remove gas produced by tissue autolysis during warming to 19 °C for either 1 h (on the first day after collection) or for 2 h (on the second day after collection). A preliminary study established that this degassing regime resulted in similar cavitation activity on both days

(McLaughlan et al. 2010). A 44-mm internal diameter, 40-mm-long, cylindrical, Perspex-framed tissue holder with 19-μm-thick acoustically transparent Mylinex windows, designed to allow unimpeded HIFU propagation along the axis of the tissue sample, simultaneous diagnostic ultrasound imaging from above and PCD monitoring from the side, was used (McLaughlan et al. 2010). Gentle compression was applied where necessary using the rear window to achieve a uniform length for all samples. The focal plane of the HIFU was set 20 mm below the capsular surface of the liver, which was always positioned facing the transducer to mimic the path through liver *in vivo*. Tissue samples were exposed only once. Exposure times of 4 s were chosen, because these were representative of those previously used in a clinical trial (Visioli et al. 1999). Three *in situ* intensities of 314, 786 and 1100 W/cm^2 (1.52, 1.77 and 1.86 MPa) were used to investigate cavitation activity in the following regimes: (i) no cavitation activity, (ii) acoustic cavitation only and (iii) acoustic cavitation plus boiling activity. HIFU beam propagation was nonlinear at all intensity levels used in this study.

Fifteen repeat measurements were made in each regime. After removal from the holder, tissue was dissected by cutting along the direction of the sound axis to reveal the lesion size and shape. The lesion was photographed under polarized light (to minimize specular reflections from the tissue surface).

RESULTS

Results are presented here in two parts: addressing degassed water and *ex vivo* tissue separately.

Degassed water experiments

Figure 2 shows typical examples of ultrasound emissions and measured drive power during 4-s HIFU exposure of degassed water at three different intensities. No ultrasonic emissions or drive power fluctuations were detected at 550 W/cm^2 (1.88 MPa). Half harmonic, broadband emissions and drive fluctuations were detected for the two exposures at 1100 (2.10 MPa) and 2200 (2.32 MPa) W/cm^2, with the amplitude and number of spikes
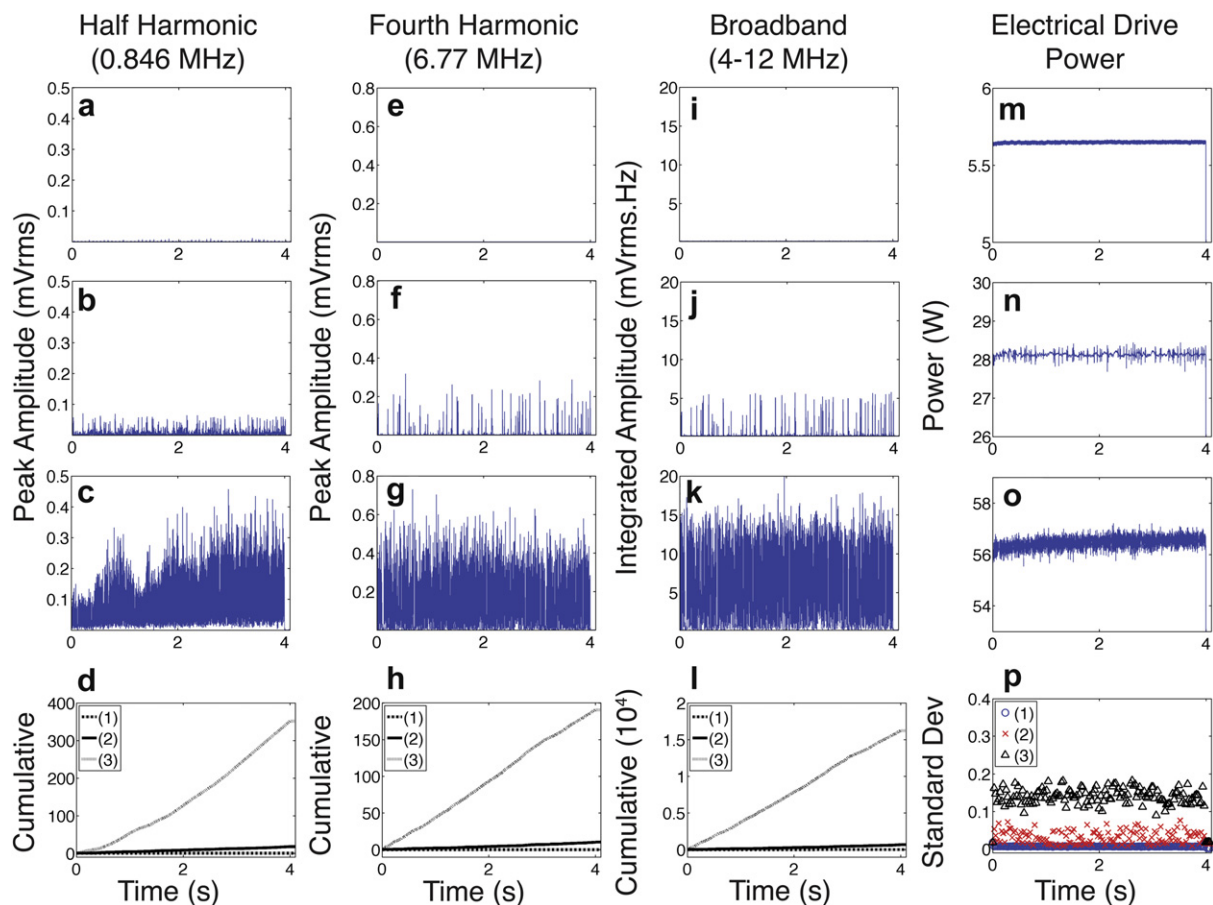

Fig. 2. Detected emissions (as labelled) and measured drive power as a function of time, acquired from three examples of 4-s HIFU exposures, quoted as in situ intensity (in situ peak-negative pressure) in degassed water at (top row) 550 W/cm^2 (1.88 MPa); (second row) 1100 W/cm^2 (2.10 MPa); and (third row) 2200 W/cm^2 (2.32 MPa). (Bottom row) The noise-corrected cumulative signals and standard deviation of the drive power fluctuations for these three exposures.

per second increasing with intensity. Even for large numbers of emissions, they appear to be discrete events, with the signal returning to background noise level between each. This was evident on an expanded time scale (McLaughlan et al. 2010). In three repeat exposures, audible emissions (with a peak centered at ∼17 kHz) were only detected at this highest exposure (McLaughlan et al. 2010). Electrical drive power fluctuations (Fig. 2n and 2o) were detected at both exposure levels. This is also shown in the plot of standard deviation (Fig. 2p); a high temporal coincidence was found between the power fluctuations, broadband emissions and the fourth harmonic signals. No such correlation was evident for the subharmonic signals, even though the low-frequency PCD focus was arranged to enclose the whole higher-frequency PCD focus (Fig. 1). The cumulative plots (Fig. 2d, 2h, 2l) show that the highest exposure level gave rise to the greatest level of detected emissions.

Ex-vivo *liver tissue experiments*

Figure 3 shows detected ultrasonic emissions, drive power fluctuations and audible emissions for each of the 4-s duration exposure regimes: (a) 314, (b) 786 and (c) 1100 W/cm^2 (1.52, 1.77 and 1.86 MPa). At 314 W/cm^2,

no half or fourth harmonic or broadband emissions were detected during the exposure, and no lesion was produced. At 786 W/cm^2, Fig. 3 (b, f, j, n) shows continuously detected half harmonic and broadband emissions above the noise level of the system. The fourth harmonic (6.77 MHz) and broadband emissions from this exposure show a slowly varying, but permanently raised, magnitude in contrast to the more transient behavior (see Fig. 2f) detected in water. However, no power fluctuations (Fig. 3n) or audible emissions (Fig. 3r) were detected. At 1100 W/cm^2 (Fig. 3c, 3g, 3k, 3o), half harmonic, fourth harmonic and broadband emissions were detected throughout the exposure, which produced the lesion shown in Fig. 4b. The regular spikes seen in the broadband emissions (Fig. 3j), which continue after the HIFU exposure, were a result of detection of the diagnostic scanner output. In the third regime, the fourth harmonic (Fig. 3g) and broadband (Fig. 3k) emissions show a significant increase in detected signal amplitude around 2.3 and 3.3 s. Corresponding fluctuations in drive power (Fig. 3o) can be seen, along with brief audible signals (Fig. 3s) in the 2–8 kHz range (indicated by a light vertical line). Figure 4b shows a larger lesion than Fig. 4a. Formed from an exposure in the third regime (1100 W/cm^2), it has
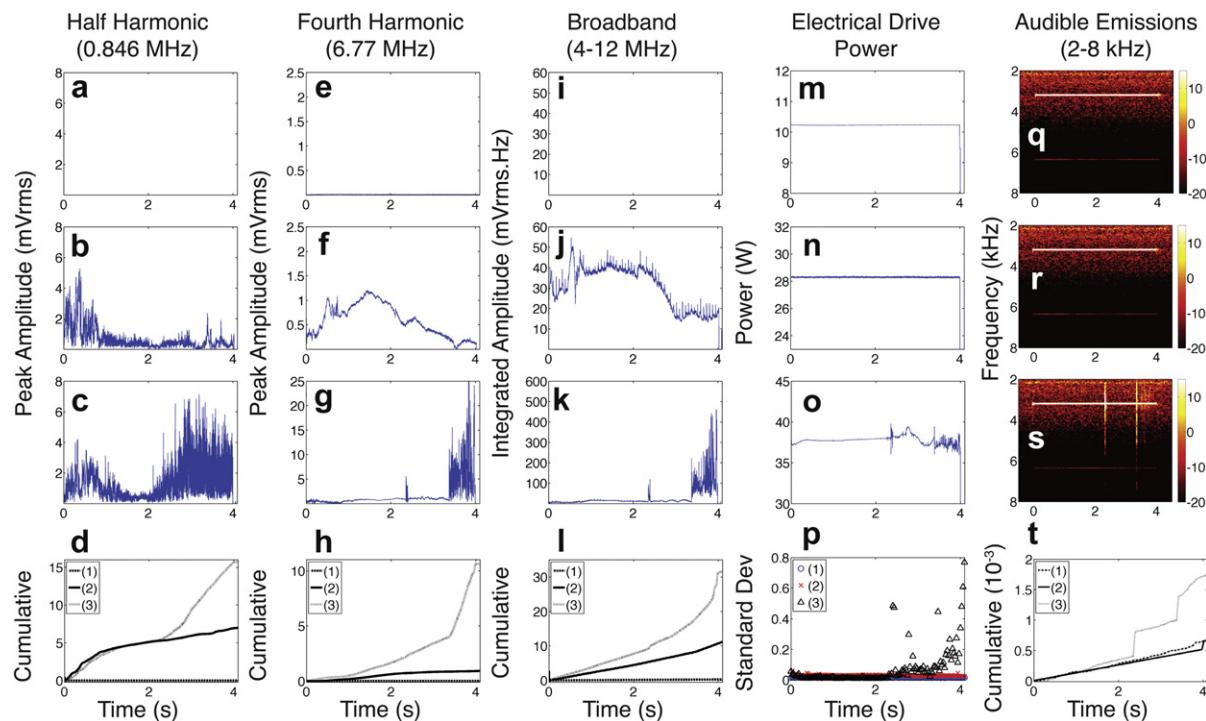

Fig. 3. Noise-corrected signals (as labelled) from 4-s HIFU exposures in each of the three cavitation regimes: (top row) 314 W/cm^2 (1.52 MPa); (second row) 786 W/cm^2 (1.77 MPa); and (third row) 1100 W/cm^2 (1.86 MPa). Note the smaller amplitudes of the detected signals compared with those from degassed water (Fig. 2), and the increased scale ranges for the highest-intensity exposure. The apparent broadband signal in (b) after HIFU exposure is a period signal from the ultrasound scanner. The noise levels of these measurements are: 0.3 ± 0.15 mVrms for half harmonic, 0.2 ± 0.03 mVrms for fourth harmonic and 0.12 ± 0.07 Vrms.Hz for broadband emissions. (Bottom row) The noise-corrected cumulative signals and standard deviation for the drive power for these three exposures.
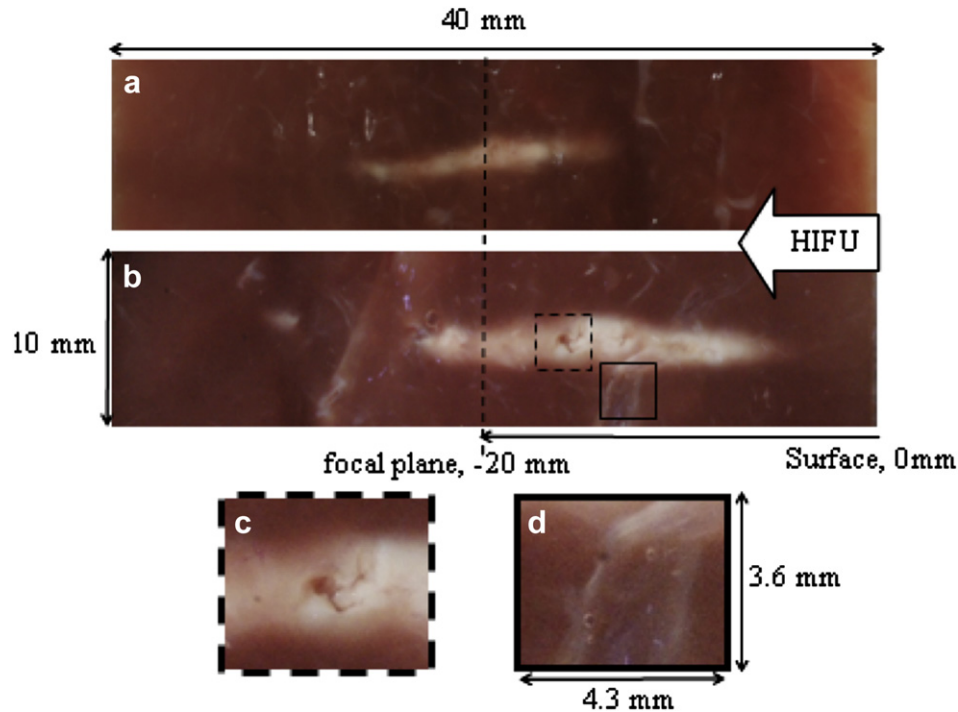
Fig. 4. Lesions generated in ex vivo bovine liver tissue at (a) 786 W/cm^2 and (b) 1100 W/cm^2 for the 4-s exposures in Fig. 3 (b and c, respectively). In both cases, the HIFU propagated from right to left. The dashed zoom box (c) shows a hole in the lesion and the solid line box (d) shows a blood vessel.

grown towards the HIFU transducer. Figure 4c shows a close-up of a "hole" caused by this exposure, which has a different appearance from that of a blood vessel (Fig. 4d).

Figure 3d shows cumulative plots of the ultrasonic emissions for the typical examples of the regimes shown in Fig. 3. The cumulative plots from the first regime do not exceed the noise level. The first 3 s of exposure show comparable levels of half harmonic in regimes 2 and 3 (Fig. 3d). However, a significant increase in the fourth harmonic (Fig. 3h), broadband (Fig. 3l) and audible emissions (Fig. 3t) detected can be seen for the third regime (acoustic cavitation and boiling) after 3s.

The average cumulative plots (Fig. 5a–5c), for the 15 exposures in each regime, show trends similar to those shown in the typical examples in Fig. 3. Figure 5d shows that power fluctuations were only significant at the highest exposure level (1100 W/cm^2) and that they occurred after ~2 s into the HIFU exposure. Averaging the cumulative plots allowed the identification of overall trends from repeated measurements of HIFU exposures in tissue.

Power fluctuations, audible emissions and hyperechogenicity were only observed in tissue during exposures at the highest intensity, as shown in Table 1. Figure 6a–6e shows five B-scan frames acquired during the 4-s, 1100-W/cm^2 exposure shown in Fig. 3 (c, g, k, o) and Fig. 4b. Each frame shows 60 mm in imaging depth and 40 mm in width, with the HIFU propagating

from right to left. Figure 6b–6d show the acoustic interface pattern seen during HIFU exposure. At 2.35 and 3.30 s, increased interference can be seen on the right side of the image (arrowed) (Fig.6c, 6d). These times coincide with detectable audible emissions (Fig. 3s). During (Fig. 6d) and after (Fig. 6e) exposure, hyperechogenic regions can be seen in the tissue in the focal region. It is possible, in this example, to see a hyperechogenic region within the HIFU interference in Fig. 6d. For comparison, Fig. 6 (f, g) shows B-mode frames obtained before and after a 314-W/cm^2 (1.52 MPa), 120-s exposure. The subtraction image, Fig. 6h, shows no apparent hyperechogenicity, even though a lesion formed (Fig. 6i). Figure 7a shows a region (boxed area in Fig. 6g) of hyperechogenicity that is larger than the HIFU focus. As shown in Table 1, hyperechogenicity was only observed in these experiments when audible emissions, such as those seen at 2.35 s and between 3.3 and 4.0 s (Fig. 3c), were recorded. Figure 7 (b, c) shows the shrinkage of the echogenic region with time (at 4.3 and 7.1 s) after HIFU exposure. Figure 6 (a–e) shows five B-mode images acquired before and during exposure but before boiling, during boiling and after a 4-s, 1100-W/cm^2 exposure. During boiling, there was an increase in the interference pattern caused by the HIFU (Fig. 6c, 6d). Frequency analysis of the radiofrequency data of the B-mode frames shown in Fig. 6 (b–d) shows that the
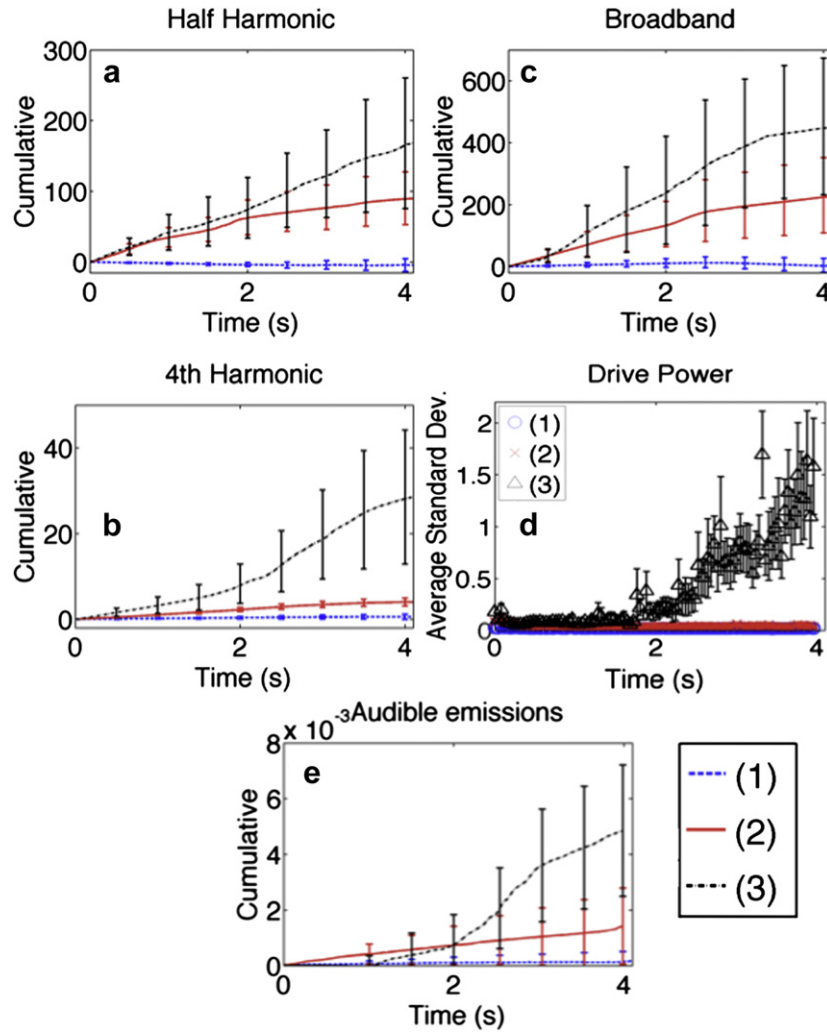
Fig. 5. (a–c) Noise-corrected averaged cumulative spectra for 15 exposures in each regime, with (1) no cavitation, (2) acoustic cavitation only and (3) acoustic cavitation and boiling. Error bars, calculated from the standard error of the mean value, are only shown at 0.5-s intervals to maintain clarity, but describe the general trend. (d) Standard deviation from the mean level of the average HIFU drive power for each exposure regime, (e) Averaged audible spectra for the three exposure regimes.

interference pattern seen is predominantly a result of the presence of the second, third and fourth harmonics generated by nonlinear HIFU propagation (Fig. 8). These integer harmonics lie within the bandwidth of the imaging array. The peak seen at 3 MHz is thought to be a signal-processing artefact. Figure 8 (c, f) shows maps of frequencies between 3–4 MHz of the frames in Fig. 6 (c, d). The highlighted region in Fig. 6e shows a large area of

Table 1. The percentage of exposures in ex vivo liver, for each regime (n = 15), where a specific indicator of cavitation was positively detected at some point during the 4-s exposure

	Fourth harmonic (%)	Fourth harmonic onset (%)	Half harmonic (%)	Integrated broadband (%)	Power fluctuations (%)	Audible emissions (%)	Hyper-echogenicity (%)
(1) No cavitation	60	0	13	0	0	0	0
(2) Acoustic cavitation	93	0	60	27	0	0	0
(3) Acoustic cavitation and boiling	100	73	100	53	100	100	84

Fourth harmonic onset is defined as occurring if the acoustic emission voltage increased by a factor of ≥10 (a minimum of 5 such events being required for a positive identification).
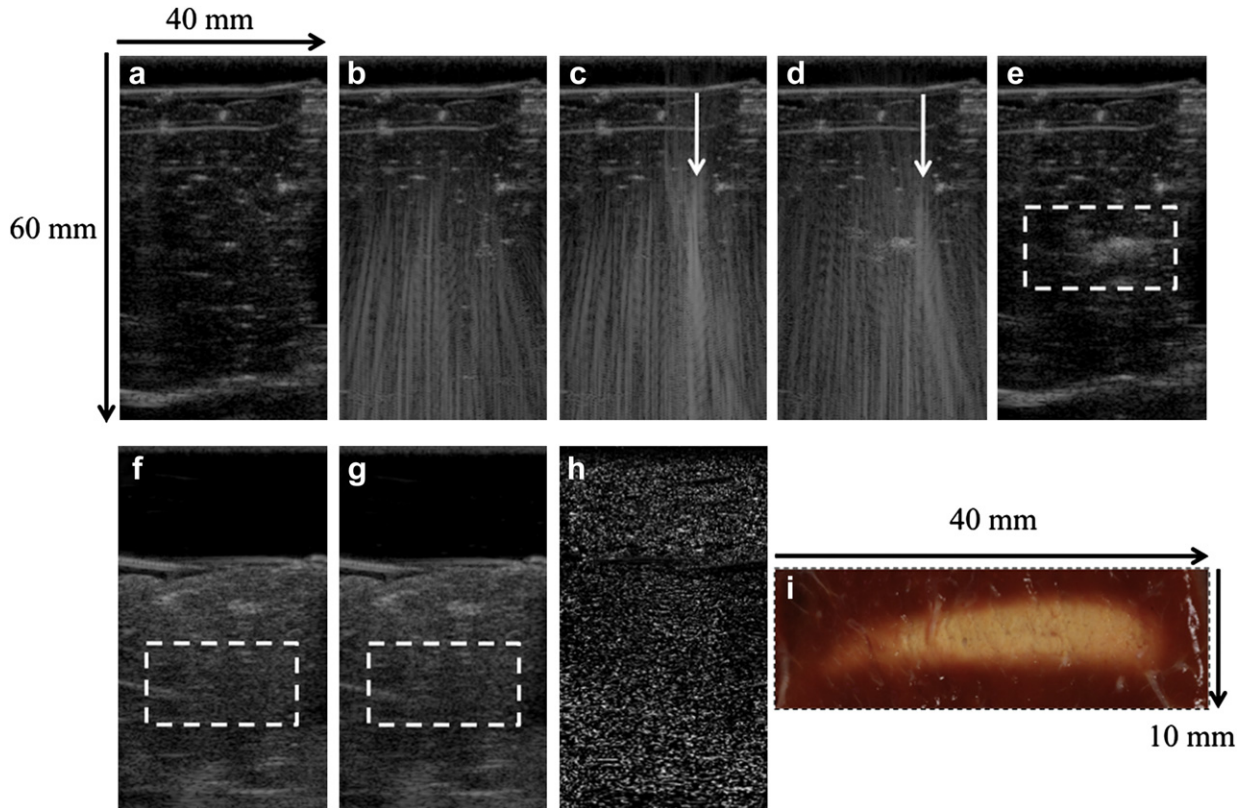
Fig. 6. (a–e) Five B-scan frames acquired with a Zonare scanner (L10.5 Probe) during the 4-s duration 1100-W/cm^2 exposure of ex vivo tissue, shown in Fig. 3c. (a) Before, (b) 2.29, (c) 2.35, (d) 3.30 s into and (e) after the HIFU exposure (timings have an uncertainty of $\pm$ 0.07 s because of the 14-Hz frame rate used). (f, g) Two B-scan frames acquired immediately before (f) and after (g) a 314 W/cm^2 120-s exposure. (h) A subtraction image showing only background noise and no echogenicity change, in the approximate position of the focal zone (indicated by the dashed white line). (i) Homogeneous lesion produced by this exposure. In all images, the HIFU propagated from right to left.

increased echogenicity, possibly associated with boiling. In the absence of the HIFU field, frequency analysis of the radiofrequency data (Fig. 6a, 6g) shows an increased scatter of the imaging beam after the exposures, corresponding to the hyperechogenicity observed in Fig. 6g and highlighted in Fig. 7. Table 1 shows the percentage of exposures for each regime in which a specific indicator was positively detected (using the criteria described earlier).

DISCUSSION

Degassed water

At 1100 W/cm^2 (Fig. 2b, 2f, 2j) and 2200 W/cm^2 (Fig. 2c, 2g, 2k), it is not possible to identify the source of the half harmonic. Although inertial cavitation was definitely present, noninertial cavitation may also have been occurring at the same time in a lower-pressure region of the bubble cloud at the periphery of the focus. Thus, both types of activity may have been occurring within
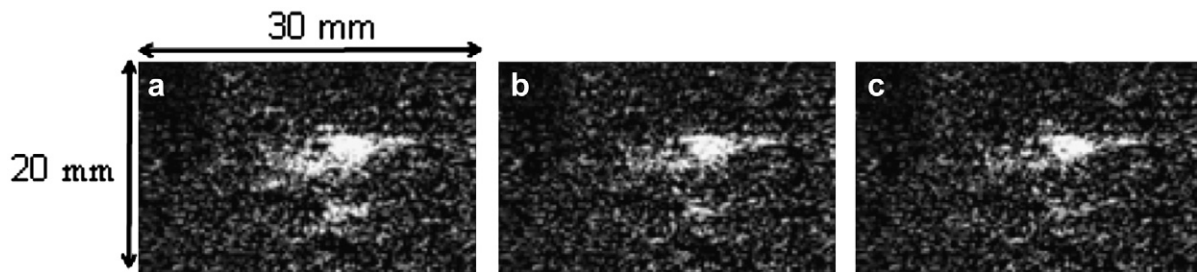

Fig. 7. Subtraction B-scan images from image frames obtained at (a) 0 s (see Fig. 6e) (b) 4.3 s and (c) 7.1 s ($\pm$ 0.07 s) after the exposure ended, indicating a decrease in the hyperechogenicity with time. The scale is the same for all images.
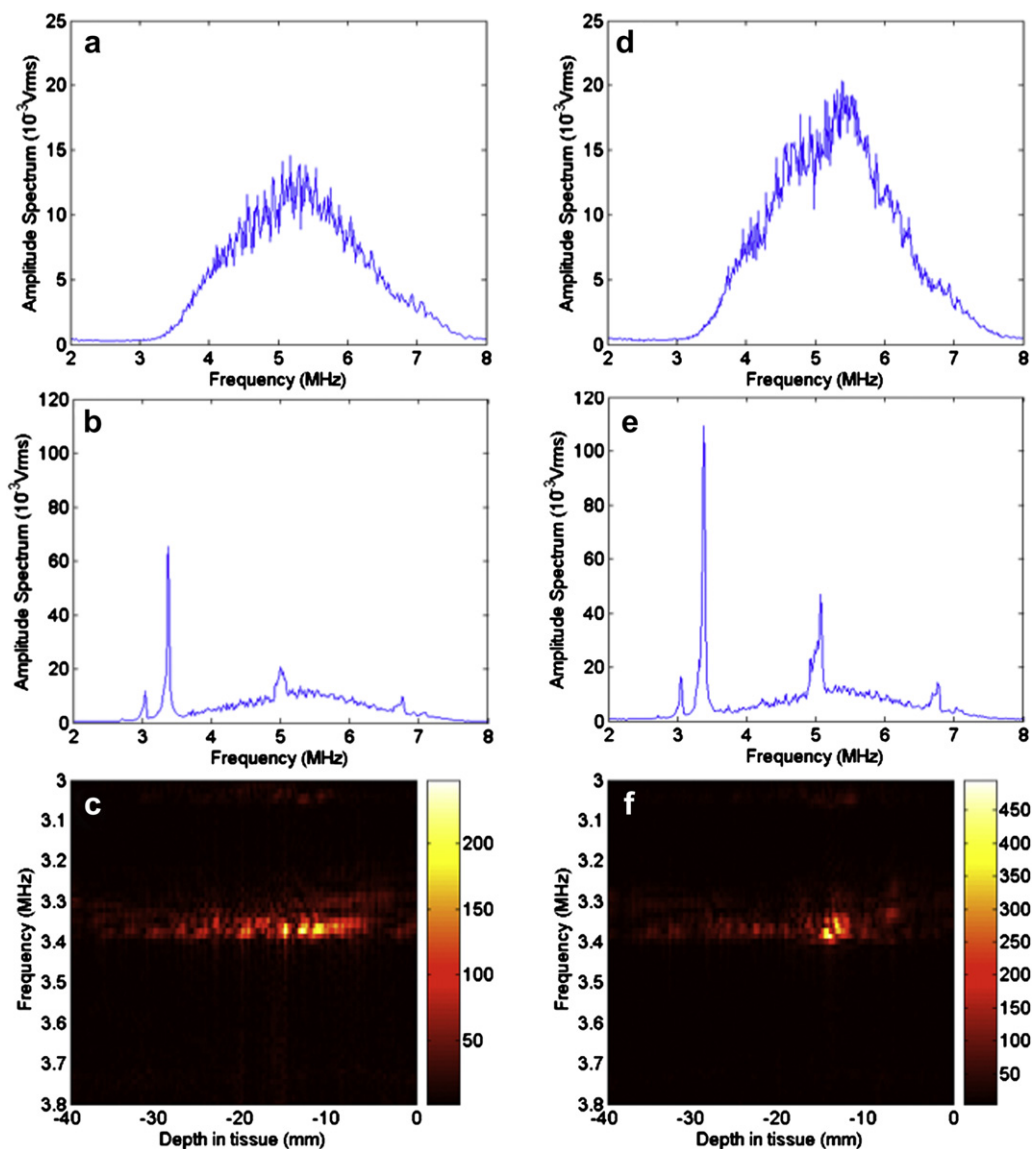
Fig. 8. Frequency spectra for B-mode images shown in Fig. 6. (a, d) were calculated from frames before and after HIFU exposure (Fig. 6a, 6e); (b) and (e) were calculated from frames acquired when the HIFU was on (Fig. 6b, 6c) with and without boiling, respectively. These were calculated by averaging the FFT spectra over a 13 × 60-mm window (i.e., image lines 90 to 160 over the full image depth). (c) and (f) show two maps of the frequency content between 3 and 4 MHz for images shown in Fig. 6: (c) is a map taken from the frame at 2.35 s (Fig. 6c, 6f) is the frame at 3.30 s (Fig. 6d) into the HIFU exposure. The scales indicate the FFT amplitude. Note the difference in amplitude between (c) and (f). The horizontal axis is the depth in the tissue sample along the HIFU sound axis at which the signal is detected (–40 mm is the first image line). The focal plane of the HIFU is at –20 mm.

the two confocally aligned PCD foci. Figure 2 (n, o) demonstrates that drive power fluctuations occurred for the two regimes that produced broadband emissions ($\geq$1100 Wcm^2), but not when half-harmonic emissions alone were detected. The same trend was found for the audible emissions ($\sim$17 kHz). This suggests that in degassed water (where HIFU cannot generate boiling bubbles) drive power fluctuations and audible emissions relate to acoustic cavitation. In particular, they are associated with inertial cavitation (broadband emissions). Drive

power fluctuations were found to coincide temporally with the detection of fourth harmonic and broadband ultrasonic emissions. Half harmonic signals showed no temporal correlation with the other signals. This suggests that inertial cavitation was required to facilitate detection of this effect in water here.

At 1100 W/cm^2 (Fig. 2b, 2f, 2j), broadband emissions are more sporadic than at 2200 W/cm^2. Closer inspection of the data (McLaughlan et al. 2010) demonstrates better temporal correlation of drive fluctuations

and audible emissions with broadband emissions than with subharmonic emissions. Thus, power fluctuations are most likely to be a result of inertial cavitation. As the intensity (peak negative pressure) is increased, detectable inertial cavitation events become statistically more probable, and a larger proportion of the focal volume of the PCD interrogates pressure regions capable of inducing acoustic cavitation, leading to both a higher rate and larger amplitude of emissions being detected.

Spectral analysis of the drive voltage and current demonstrates that only the fundamental drive frequency was present, probably because of the limited bandwidth of the HIFU transducer. This suggests that the power fluctuations were caused predominantly by the backscatter of the fundamental frequency from cavitation bubbles (McLaughlan et al. 2010).

Ex vivo *tissue experiments*

Interpretation of the results obtained in tissue is significantly more complicated than for a liquid. First, ultrasound energy absorption in tissue leads to heating and to thermal gradients across the HIFU focal region. Not only will this affect acoustic cavitation nucleation, but, as the temperature approaches 100 °C, intra- and extracellular water may undergo thermally-driven gas space formation ("boiling") from the vapourization of liquid and the exsolution of formerly dissolved permanent gas out of the liquid and into gas spaces. Second, the attenuation and absorption coefficients of most tissues (including liver, but not fat) increase with frequency, affecting higher-frequency ultrasonic emissions much more than those at lower frequency. Finally, although it has for years been accepted that inertial cavitation in living human tissue might be expected to be less easy to generate than for the same insonification conditions in water, experimental verification of this in living humans is sparse (the first being Leighton et al. 1990). Even today, most studies compare water with excised animal tissue. It is generally accepted that a reduced number of nucleation sites, and the effect of tissue on the individual bubble dynamics (depending on the tissue in question), are significant contributors to this difference.

Passive cavitation detection

The PCD acoustic cavitation activity indicators (half and fourth harmonics and broadband emissions) in tissue were noticeably different from those observed in water. The kurtosis is different, most noticeably in the fourth harmonic and broadband datasets; although water generated discrete spikes rising from a lower baseline (Fig. 2), tissue produced a continuously raised level, with discrete spikes extending above it (Fig. 3). The reason for the apparently continuous activity in tissue might be the raised tissue temperature, facilitating

increased cavitation nucleation; the tissue structures and viscosity prevent cavitation bubbles from streaming out of the detector foci. These observed differences in signal patterns suggest that it might be possible to understand the complex situation that occurs at water/tissue interfaces. Tissue can of course constrain bubble dynamics in a way that cavitation in free-field aqueous conditions cannot (Leighton et al. 1995; Sassaroli and Hynynen 2007; Vykhodtseva et al. 2008; Martynov et al. 2009; Jang et al. 2009) and this provides another potential source of difference between the aqueous and in-tissue results.

Unlike in degassed water, audible emissions and power fluctuations (Fig. 3) were not detected in tissue in the presence of acoustic cavitation unless boiling occurred (Table 1). One reason for this difference could be that tissue attenuated the drive signal backscatter too strongly to cause detectable power fluctuations. A more likely explanation is a lack of cavitation nucleation sites, and thus insufficient numbers of bubbles to produce detectable backscatter of the HIFU field in tissue. For 1100-W/cm^2 (1.86 MPa) 4-s exposures, power fluctuations and audible emissions (Fig. 3) were detected simultaneously after 2.3 s, suggesting that boiling bubbles gave rise to sufficient backscatter to generate detectable power fluctuations. Boiling events may occur at different locations within the focus (Fig. 8c, 8f) at different times. This may explain the break in the audible emissions seen between 2.3 and 3.3 s (Fig. 3s). However, it should be noted that, as seen in Fig. 8 (c, f) the largest scattering event occurred outside the focal region of the PCDs, which were centered at 20 mm below the tissue surface. However, signals were detected by the PCD, because it is possible that the boiling event acted as a strong nucleation source for acoustic cavitation. One potential problem when combining both simultaneous PCD and ACD, highlighted in Fig. 3j, arises from the overlap in bandwidth of the diagnostic imaging system and the sensor used for the PCD.

No statistically significant cavitation activity was detectable above the noise in the averaged cumulative plots (n = 15) shown in Fig. 5, for the lowest intensity ("no cavitation") exposure regime. For emissions in the "acoustic cavitation" regime, the error bars are significantly greater than those in the absence of cavitation, presumably because of its statistical nature. Nevertheless, there is a statistically significant increase above noise in signal accumulation when acoustic cavitation occurs, as demonstrated by the cumulative half harmonic and broadband emissions in Fig. 5 (a, c). For the boiling regime, the initial similarity with the acoustic cavitation curve suggests that this dominates broadband emissions up to around 2 s, the point at which boiling begins to occur under these exposure conditions. Boiling results in a further increase in broadband emissions, with the

cumulative value at 4 s being approximately twice that for acoustic cavitation only. This also results in a near doubling in the size of the error bars. Boiling bubbles are likely to be too large to undergo inertial collapse (Leighton 2007) and so are unlikely to generate broadband emissions in the 4–12-MHz band (other mechanisms, e.g., bursting, might generate broadband at lower frequencies). However, boiling bubbles may influence the 4–12-MHz broadband signal indirectly by generating nuclei for inertial cavitation. The effect of boiling on the cumulative fourth harmonic is even more dramatic than for the broadband emissions. Here, the larger cumulative value seen before 2 s, compared with the other regimes at lower pressures, is caused by greater nonlinear propagation of the HIFU beam. The averaged power fluctuations and audible emissions (Fig. 5d, 5e) show an increase after approximately 2 s only for the "boiling" regime.

Table 1 shows the percentage of exposures for which there was a positive indication of cavitation activity at some point during exposure. In the first regime (no cavitation), some fourth harmonic was detected in 60% of the exposures, but was not sufficiently long lasting to allow determination of an "onset" time. This was therefore believed to be generated by nonlinear propagation in the tissue, and to have been scattered by inhomogeneities in the sample (McLaughlan et al. 2010). The variation in scattering between tissue samples may explain why the fourth harmonic is sometimes not seen. However, the relatively small error bars in Fig. 5b demonstrate that this variation is small compared with variations as a result of bubble activity. Half harmonic was only detected in ~13% of these low-intensity exposures, suggesting that this exposure level (314 W/cm^2 or 1.52 MPa) may be close to the lowest negative pressure required to generate noninertial cavitation. This highlights a potential difficulty when trying to specify cavitation thresholds in tissue precisely. As intensity was increased, half harmonic was detected in 0, 60 and 100%, and integrated broadband was detected in 0, 27 and 53% of the exposures in the three regimes. Difficulty in detection of broadband emissions may be caused by attenuation of these signals (4 to 12 MHz) in tissue, whereas this is less significant for the half-harmonic emissions. The fourth harmonic was readily detected in all of the three exposure regime, highlighting the need to filter out nonlinear harmonics when integrating broadband emissions. Nevertheless, fourth harmonic "onset" time was measurable in 73% of the exposures in the third regime, corresponding to the only exposure conditions that resulted in the sudden appearance of a hyperechoic region on the B-mode image (McLaughlan et al. 2010), i.e., a boiling event. In these experiments, the HIFU focus was only 20 mm deep in tissue. These devices cannot be located in clinically relevant positions relative to the HIFU source because

of their relatively short focal lengths. They were used to investigate which monitoring techniques showed promise, rather than to inform the design of specific sensors for clinical use. A disadvantage of using multiple single-element confocal detectors with different sensing volumes (not discussed in this paper) is the ambiguity in identifying from where the emissions emanate. This could be addressed through the use of a PCD array (Farny et al. 2009). Power fluctuation and audible emissions occurred only at the highest exposure level, for 100% of the 15 exposures.

Audible emissions, power fluctuations and boiling

Table 1 and the cumulative data (Fig. 5e) demonstrate the consistent simultaneous increase in broadband signals, appearance of transient audible emissions (2 to 8 kHz) and transient or sustained drive power fluctuation. It was found that audible emissions in tissue caused by acoustic cavitation were generally transient and broadband (below <10 kHz), whereas in degassed water, emissions contained a more discrete frequency component, centered around ~17 kHz. Broadband ultrasonic signals may not be emitted by boiling bubbles; rather, it is more likely that these bubbles generate gas nuclei, which then undergo inertial cavitation. It has long been recognized that cavity collapses may be cushioned by vapour as well as dissolved gas (Leighton 1994; Matula et al. 2002), and if boiling is occurring during HIFU, temperatures will approach 100 °C and therefore vapour pressures may be high enough to restrict violent collapse. However, although the negative pressure at 1100 W/cm^2 was 1.86 MPa, the positive pressure was 7.63 MPa. Solution of the Rayleigh-Plesset equation (Leighton 1994) suggests, within the limitations of this model, that at this peak positive pressure and elevated temperature, a bubble can still collapse. Figure 9 shows that as the exposure intensity is increased, audible emissions occurred earlier in the exposure. This is consistent with the hypothesis that these are resultant from boiling, in that higher intensities would cause faster temperature rise, resulting in boiling occurring earlier in the exposure, and with the formation of gas bodies, which, through scatter, cause local increases in the drive pressure above the levels expected in the free field (Leighton 2007; Coussios and Roy 2008).

The increase in the interference pattern was shown to be caused predominantly by the scattering of the superharmonics of the HIFU beam (Fig. 8b, c). It was assumed that boiling occurred in the plane of the HIFU beam axis. Figure 8c shows a map of the HIFU second harmonic detected by the diagnostic scanner in the first frame acquired after tissue boiling. Analysis over a wider frequency band revealed no extra information. The depth of the maximum signal beneath the tissue surface (in the direction of HIFU
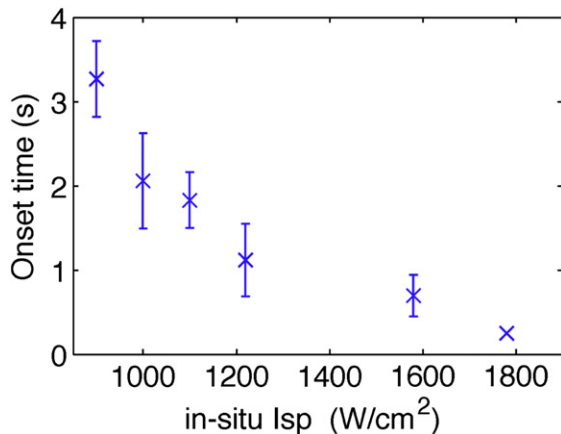
Fig. 9. The average time for the first occurrence of audible emissions in ex vivo bovine liver exposed to HIFU for 4-s HIFU exposures targeted 20 mm deep in tissue, showing a decrease in the time at which audible emissions occurred with the HIFU intensity. n = 3–17 on the data points with error uncertainty bars (s.d.), n < 3 for the points without.

propagation) is approximately 15 mm, corresponding to the position at which a hole was found in the lesion on subsequent dissection (Fig. 4c). This suggests that the boiling event occurring at ~2.35 s caused this tissue damage. Because this occurred on the HIFU axis ahead of the foci of both passive cavitation detectors, they might be expected to be insensitive to this event. However, this was not the case, indicating that boiling must produce ultrasonic emissions (Fig. 3) of sufficient amplitude to be detectable under these circumstances. The boiling and broadband emissions probably coincided spatially because if they did not, the boiling bubbles might be expected to shield the foci of the PCDs (Leighton 1995; Thomas et al. 2005; Khokhlova et al. 2006), causing a drop in intensity (pressure) and thus a reduction in broadband emissions. This was not seen. However, simple explanations and extrapolations between water, phantoms and tissue are difficult with respect to shielding because the formation, movement, effectiveness and disintegration of bubble shields is a complicated phenomenon that depends on the local dissolved gas content, fluid viscosity and temperature; the ability of gas pockets to migrate; and the duration of exposure and pulsing regimes (Pickworth et al. 1988).

Hyperechogenic tissue regions were only seen for exposures during which audible emissions and drive fluctuations had been detected. The example in Fig. 7d shows hyperechogenicity throughout the HIFU interference as well as after the exposure. The lesion shown in Fig. 4b is not well represented spatially by the hyperechogenic region seen in Fig. 7a, because it overestimates lesion size. This could be caused by scatter from bubbles outside the visible lesion volume or because of imaging artefacts

resulting from particularly strong echoes from boiling bubbles within the lesion. Broadband emissions also increased at this time (Fig. 3c), suggesting an increase in the inertial cavitation activity. Although Khokhlova et al. (2006) demonstrated that acoustic cavitation in scatterer-free gels could be a source of echogenicity in B-mode images (before the onset of boiling), we were unable to observe such an effect in ex vivo liver. This is likely to be a result of the background scatter of the liver creating a high detection level noise floor. In our study, although the hyperechogenicity persisted for many seconds after the exposure, it shrank (Fig. 7b, 7c). This is consistent with the hyperechogenicity observed in gel by Khokhlova et al. (2006) after boiling. This time scale means that the size reduction is more likely to be a result of tissue cooling and condensation of vapour into a liquid than to dissolution of micron-sized bubbles (Bailey et al. 2001). Any permanent hyperechogenicity would arise from scatter from boundaries created within the lesion, such as the hole seen in Fig. 4c.

Recommendations for development of a clinical cavitation detection system

In the clinic, monitoring of drive power fluctuations could be the easiest of the techniques described here to implement. However, at clinical treatment depths, attenuation of the scattered drive signal will reduce detection sensitivity. The monitoring of audible emissions in a clinical environment may be difficult, because of respiration and cardiac noise within the patient. However, judicious placement of a microphone may allow these to be monitored effectively. This technique could provide instantaneous feedback about boiling events and could be compared with B-mode imaging after the exposure. (The appearance of hyperechoic regions on a B-scan is the current clinical "gold standard" for identifying tissue ablation). Although both techniques require further investigation, real-time monitoring with the aim of detecting the start of boiling during treatment could aid treatment planning and delivery. Active cavitation detection provides useful indication of the onset of boiling during exposures, manifesting itself as increased HIFU interference in B-mode images. It was possible to identify hyperechogenic regions in B-mode images (preferably using subtraction) obtained immediately after HIFU exposures in which boiling occurred. Real-time B-mode monitoring of hyperechoic regions requires interleaving of HIFU and imaging exposures. We have demonstrated that hyperechogenicity may coincide with holes produced within lesions because of boiling activity. However, it is not possible to determine from this study what effect the bulk increase in temperature occurring during the HIFU exposure has on these cavitation activity regimes. Boiling bubbles result in lesion growth towards the HIFU

transducer. Whether this is caused by boiling bubbles directly or by their potential to act as catalysts for seeding acoustic cavitation remains to be seen. These are areas for future study. Similarly, we have not assessed our specific sensors for clinical use. Clearly the PCD sensors are likely to have too short a focal length for HIFU treatment depths exceeding 4 cm. Because there will be more attenuation at greater depths and the emissions will scatter into a greater solid angle, it is likely that devices suitable for clinical use will require both longer focal lengths and wider apertures in an attempt to retain sensitivity. It may be better to select a lower-frequency band for integration of broadband emissions. This may also reduce the size of the focal region, potentially increasing spatial specificity.

CONCLUSIONS

A suite of techniques that allows simultaneous monitoring of the highly transient cavitation activity seen during HIFU exposures has been described. The novelty resides in the use not only of the standard combination of PCD (1 to 20 kHz and 0.1 to 12 MHz) and ACD (Zonare scanner) measurements, but also in the simultaneous monitoring of both audible emissions and HIFU drive power fluctuations. It has been demonstrated that these techniques are not without interaction, because the HIFU signals interfere with ACD, and the ACD produces noise that is detected by the PCD.

When cavitation occurs at a water/tissue interface (e.g., water/skin or bladder/urine), the complex events that occur may be best understood using an extensive suite of detection capability. This proposition is based on the observed differences between indicators of acoustic cavitation (half and fourth harmonics and broadband emissions) in water and tissue (in terms of kurtosis and baseline levels). We have also shown that power fluctuations, which were found to coincide temporally with the incidence of fourth harmonic and broadband signals, were only detected in degassed tap water at drive levels that produced inertial cavitation.

The construction of noise-corrected cumulative plots provided not only an additional, useful method of comparing emissions between exposures, but also a technique for studying trends. Monitoring the accumulation of emissions during a clinical exposure warrants investigation to determine whether it is an appropriate method for control of exposure conditions based on feedback from cavitation activity. Although it would be unlikely that this method could give useful information on a "shot-by-shot" basis, such an analysis might be useful in highlighting the role, if any, acoustic cavitation has in the formation of lesions in the clinical setting. Finely sampled temporal data from similar exposures were averaged without overinterpretation of minor temporal variation

of, e.g., the onset time of boiling or a change in acoustic cavitation activity. Averaging of cumulative data shows the same clear differentiation between the different regimes of thermal and mechanical exposure as demonstrated by the temporal detection data in Table 1. This suggests that this new approach could be useful for monitoring clinical cavitation and/or providing feedback during treatment.

In degassed ex vivo bovine liver, boiling was always associated with a dramatic increase in transient audible emissions (over the range 2 to 8 kHz), drive power fluctuations and, in 84% of cases, ultrasound image hyperechogenicity (Table 1). Fourth harmonic emissions were present even in the absence of subharmonic and were attributed to scatter of the nonlinear components of the HIFU field. However, for only 73% of exposures in which boiling was observed did a rapid increase in the "onset" of the detected harmonic occur. This was consistent with the sudden presence of a large scattering site. Thus, the monitoring of harmonics scattered in the tissue could provide useful real-time indication of a boiling event. In addition, even though no direct boiling mechanism can generate an increase in broadband emission, this was observed. This was assumed to be the result of an increase in nucleation sites resulting from boiling activity.

Using our full suite of simultaneous detection techniques, it was possible to confirm our categorization of HIFU exposures into three types:

(i) purely thermal exposure (i.e., no acoustic or audible emissions, power fluctuations or hyperechogenicity detected);
(ii) thermal exposure with acoustic cavitation (i.e., half harmonic with or without simultaneous broadband emissions, but no hyperechogenicity or audible signals detected); and
(iii) thermal exposures with acoustic cavitation and thermally driven gas space formation (i.e., audible and all ultrasonic emissions plus power fluctuations and hyperechogenicity [during and/or after HIFU exposure] detected).

Our 4-s exposure duration ex vivo liver study identified the regimes, quoted in terms of in situ intensity (pressure), for generating the above exposure regimes as (i) 314 W/cm^2 ± 10% (1.52 MPa ± 7%), (ii) ≥786 W/cm^2 ± 10% (1.77 MPa ± 7%) and (iii) >1100 W/cm^2 ± 10% (1.86 MPa ± 7%). Note that these all fall below the levels suggested for successful clinical ablation (Visioli et al. 1999).

This "full-spectrum" approach allowed both a better understanding of, and differentiation between, cavitation activities and a preliminary assessment of which of these

techniques might have the most clinical potential. In the clinical situation, boiling would be the most easily detected, because of the ease of measurement of drive power fluctuations. Audible emissions (2 to 8 kHz) that were solely a result of boiling will propagate with only low absorption, scattering and directionality through tissue and could provide a robust clinical indicator providing strategies are in place to distinguish the boiling component from ambient noise (such as those caused by respiration and heart beat). Therefore, any, or all three, of these techniques have clinical potential worthy of further investigation to identify sensors that could be used. When hyperechogenity occurred in the B-mode images, we were able to use it to identify the location of boiling events during exposure. This required an assumption that the events were within the focal region, lying along the sound axis. Although detection of broadband ultrasonic emissions proved to be the most sensitive technique for monitoring inertial cavitation in this study, in the clinical situation, the range of usable frequencies will be modified by such frequency-dependent features as the attenuation of tissue, scattering by anatomical features in the propagation path and the directionality of acoustic detectors of a given size. Where exposures occur at a water/tissue interface, we have demonstrated that it is only in water that inertial cavitation leads to power fluctuations (and increased fourth harmonic), unless boiling occurs within the tissue. This ex vivo study indicates where further knowledge is required for the design of a clinically useful system. Our ''full spectrum'' cavitation detection system, once optimized, may be suitable for future implementation of real-time monitoring in vivo, and if acoustic cavitation activity can be used to improve treatment delivery, it might be useful in a controlled feedback loop to achieve bubble-enhanced HIFU treatments.

REFERENCES

Anand A, Kaczkowski PJ. Monitoring formation of high intensity focused ultrasound (HIFU) induced lesions using backscattered ultrasound. Acoust Res Lett Online 2004;5:88–94.

ANSI Technical Report. Bubble detection and cavitation monitoring. ANSI S1.24 TR-2002. 2002:80.

Bailey MR, Couret LN, Sapozhnikov OA, Khokhlova VA, ter Haar G, Vaezy S, Shi X, Martin R, Crum LA. Use of overpressure to assess the role of bubbles in focused ultrasound lesion shape in vitro. Ultrasound Med Biol 2001;27:695–708.

Bailey MR, Khokhlova VA, Sapozhnikov OA, Kargl SG, Crum LA. Physical mechanisms of the therapeutic effect of ultrasound [review].

Acoust Phys 2003;49:369–388 (Translated from Akusticheskiĭ Zhurnal 2003;49:437–464).

Birkin PR, Power JF, Vincotte AML, Leighton TG. A 1kHz resolution frequency study of a variety of sonochemical processes. Phys Chem Phys 2003;5:4170–4174.

Canney MS, Khokhlova VA, Bessonova OV, Bailey MR, Crum LA. Shock-induced heating and millisecond boiling in gels and tissue due to high intensity focused ultrasound. Ultrasound Med Biol 2010;36:250–267.

Chen WS, Brayman AA, Matula TJ, Crum LA. Inertial cavitation dose and hemolysis produced in vitro with or without Optison. Ultrasound Med Biol 2003;29:725–737.

Chitnis PV, Cleveland RO. Quantitative measurements of acoustic emissions from cavitation at the surface of a stone in response to a lithotripter shock wave. J Acoust Soc Am 2006;119: 1929–1932.

Coakley WT. Acoustical detection of single cavitation events in a focused field in water at 1 MHz. J Acoust Soc Am 1971;49:792–801.

Coleman AJ, Choi MJ, Saunders JE, Leighton TG. Acoustic emission and sonoluminescence due to cavitation at the beam focus of an electrohydraulic shock wave lithotripter. Ultrasound Med Biol 1992;18: 267–281.

Coussios CC, Farny CH, Haar GT, Roy RA. Role of acoustic cavitation in the delivery and monitoring of cancer treatment by high-intensity focused ultrasound (HIFU). Int J Hyperthermia 2007;23:105–120.

Coussios CC, Roy RA. Applications of acoustics to non-invasive therapy and drug delivery. Annu Rev Fluid Mech 2008;40: 395–420.

Crum LA, Law W. The relative roles of thermal and nonthermal effects in the use of high intensity focused ultrasound for the treatment of benign prostatic hyperplasia. ICA 95 committee. Proceedings of the 15th International Congress on Acoustics Trondheim, Norway 1995;3:315–318.

Deng CX, Xu Q, Apfel RE, Holland CK. In vitro measurements of inertial cavitation thresholds in human blood. Ultrasound Med Biol 1996; 2:939–948.

Duck FA. Acoustic properties of tissues at ultrasonic frequencies. In: Physical properties of tissues. A comprehensive reference book. London: Academic Press Ltd; 1990:73–124

Everbach EC, Makin IR, Azadniv M, Meltzer RS. Correlation of ultrasound-induced hemolysis with cavitation detector output in vitro. Ultrasound Med Biol 1997;23:619–624.

Farny CH, Holt RG, Roy RA. Temporal and spatial detection of HIFU-induced inertial and hot-vapor cavitation with a diagnostic ultrasound system. Ultrasound Med Biol 2009;35:603–615.

Filonenko EA, Khokhlova VA. Effect of acoustic nonlinearity on heating of biological tissue by high-intensity focused ultrasound. Acoust Phys 2001;47:468–475 (Translated from Akusticheskiĭ Zhurnal 2001; 47:541–549).

Hill CR, Rivens I, Vaughan MG, terHaar GR. Lesion development in focused ultrasound surgery—A general-model. Ultrasound Med Biol 1994;20:259–269.

Holland CK, Deng CX, Apfel RE, Alderman JL, Fernandez LA, Taylor KJ. Direct evidence of cavitation in vivo from diagnostic ultrasound. Ultrasound Med Biol 1996;22:917–925.

Hwang JH, Tu J, Brayman AA, Matula TJ, Crum LA. Correlation between inertial cavitation dose and endothelial cell damage in vivo. Ultrasound Med Biol 2006;32:1611–1619.

Hynynen K. The threshold for thermally significant cavitation in dog's thigh muscle in vivo. Ultrasound Med Biol 1991;17: 157–169.

Illing RO, Leslie TA, Kennedy JE, Calleary JG, Ogden CW, Emberton M. Visually directed high-intensity focused ultrasound for organ-confined prostate cancer: A proposed standard for the conduct of therapy. BJU Int 2006;98:1187–1192.

Jang NW, Gracewski SM, Abrahamsen B, Buttaccio T, Halm R. Natural frequency of a gas bubble in a tube: Experimental and simulation results. J Acoust Soc Am 2009;126:EL34–EL40.

Kennedy JE. High-intensity focused ultrasound in the treatment of solid tumours. Natl Rev Cancer 2005;5:321–327.

Khokhlova VA, Bailey MR, Reed JA, Cunitz BW, Kaczkowski PJ, Crum LA. Effects of nonlinear propagation, cavitation, and boiling in lesion formation by high intensity focused ultrasound in a gel phantom. J Acoust Soc Am 2006;119:1834–1848.

Khokhlova TD, Canney MS, Donghoon L, Marro KI, Crum LA, Khokhlova VA, Bailey MR. Magnetic resonance imaging of boiling induced by high intensity focused ultrasound. J Acoust Soc Am 2009;125:2420–2431.

Leighton TG, Pickworth MJ, Tudor J, Dendy PP. A search for sonoluminescence in vivo in the human cheek. Ultrasonics 1990;28:181–184.

Leighton TG. The acoustic bubble. London: Academic Press; 1994. 87–93, 294–296, 302–304.

Leighton TG, White PR, Marsden MA. Applications of one-dimensional bubbles to lithotripsy, and to diver response to low frequency sound. Acta Acoustica 1995;3:517–529.

Leighton TG. Bubble population phenomena in acoustic cavitation. Ultrasonics Sonochem 1995;2:S123–S136.

Leighton TG, Phelps AD, Ramble DG, Sharpe DA. Comparison of the abilities of eight acoustic techniques to detect and size a single bubble. Ultrasonics 1996;34:661–667.

Leighton TG, Birkin PR, Hodnett M, Zeqiri B, Power JF, Price GJ, Mason T, Plattes M, Dezhkunov N, Coleman AJ. Characterisation of measures of reference acoustic cavitation (COMORAC): An experimental feasibility trial. In: Bubble and particle dynamics in acoustic fields: Modern trents and applications. Kerala, India: Research Signpost 2005;37–94.

Leighton TG, Fedele F, Coleman A, McCarthy C, Ryves S, Hurrell A, De Stefano A, White PR. A passive acoustic device for real-time monitoring the efficacy of shockwave lithotripsy treatment. Ultrasound Med Biol 2008;34:1651–1665.

Leighton TG. What is ultrasound? Progr Biophys Mol Biol 2007;93: 3–83.

Martynov S, Stride E, Saffari N. The natural frequencies of microbubble oscillation in elastic vessels. J Acoust Soc Am 2009;126:2963–2972.

Mast D, Salgaonkar V, Karunakaran C, Besse J, Datta S, Holland C. Acoustic emissions during 3.1 MHz ultrasound bulk ablation in vitro. Ultrasound Med Biol 2008;34:1434–1448.

Matula TJ, Hilmo PR, Storey BD, Szeri AJ. Radial response of individual bubbles subjected to shock wave lithotripsy pulses in vitro. Phys Fluids 2002;14:913–921.

McLaughlan JR, Rivens IH, ter Haar GR, Shaw A, Leighton T, Humphrey V, Birkin P, Vian C. The design and implementation of a passive cavitation detection system for use with ex vivo tissue. 5th International Symposium on Therapeutic Ultrasound, Melville, New York 2006:338–342.

McLaughlan J, Rivens I, ter Haar G. Cavitation detection in ex vivo bovine liver tissue exposed to high intensity focused ultrasound (HIFU). 4th IEEE International Symposium on Biomedical Imaging: From Nano to Macro 2007;1124–1127.

McLaughlan JR, Rivens I, ter Haar G. A study of cavitation activity in ex-vivo tissue exposed to high intensity focused ultrasound. 6th International Symposium on Therapeutic Ultrasound, Melville, New York 2007b:178–184.

McLaughlan J, Rivens I, Leighton TG, ter Haar G. Commentary on the detection of bubble activity generated in ex-vivo tissue by high intensity focused ultrasound (HIFU) with respect to the generation of therapeutic lesions in tissue for the treatment of cancer. ISVR Technical Report 330 (2010). Available at: http://www.isvr.soton.ac.uk/fdag/ HIFU.HTM.

Meaney PM, Cahill MD, ter Haar GR. The intensity dependence of lesion position shift during focused ultrasound surgery. Ultrasound Med Biol 2000;26:441–450.

Medwin H. Counting bubbles acoustically: A review. Ultrasonics 1977; 15:7–13.

Melodelima D, Chapelon JY, Theillere Y, Cathignol D. Combination of thermal and cavitation effects to generate deep lesions with an endocavitary applicator using a plane transducer: Ex vivo studies. Ultrasound Med Biol 2004;30:103–111.

Miller DL. Ultrasonic detection of resonant cavitation bubbles in a flow tube by their second-harmonic emissions. Ultrasonics 1981;19: 217–224.

Neppiras EA, Coakley WT. Acoustical cavitation in a focused field in water at 1 MHz. J Sound Vibr 1979;45:341–373.

Neppiras EA. Acoustic cavitation. Phys Lett 1980;61:159–251.

Neppiras EA. Acoustic cavitation series. 1. Acoustic cavitation—An introduction. Ultrasonics 1984;22:25–28.

Pickworth MJW, Dendy PP, Leighton TG, Walton AJ. Studies of the cavitational effects of clinical ultrasound by sonoluminescence: 2 thresholds for sonoluminescence from a therapeutic ultrasound beam and the effect of temperature and duty cycle. Phys Med Biol 1988;33:1249–1260.

Poliachik SL, Chandler WL, Mourad PD, Bailey MR, Bloch S, Cleveland RO, Kaczkowski P, Keilman G, Porter T, Crum LA. Effect of high-intensity focused ultrasound on whole blood with and without microbubble contrast agent. Ultrasound Med Biol 1999;25: 991–998.

Rabkin BA, Zderic V, Vaezy S. HIFU-induced hyperecho in ultrasound images, cavitation activity and thermal behavior. 4th International Symposium on Therapeutic Ultrasound, Melville, New York 2005;754:43–46.

Rabkin BA, Zderic V, Crum LA, Vaezy S. Biological and physical mechanisms of HIFU-induced hyperecho in ultrasound images. Ultrasound Med Biol 2006;32:1721–1729.

Roy RA, Madanshetty SI, Apfel RE. An acoustic backscattering technique for the detection of transient cavitation produced by microsecond pulses of ultrasound. J Acoust Soc Am 1990;87: 2451–2458.

Sanghvi NT, Fry FJ, Bihrle R, Foster RS, Phillips HM, Syrus J, Zaitsev A, Hennige C. Microbubbles during tissue treatment using high intensity focused ultrasound. Proceedings of IEEE 95 UFFC Symposium 1995;1249–1253.

Sassaroli E, Hynynen K. Cavitation threshold of microbubbles in gel tunnels by focused ultrasound. Ultrasound Med Biol 2007;33: 1651–1660.

Silverman RH, Muratore R, Ketterling JA, Mamou J, Coleman DJ, Feleppa EJ. Improved visualization of high-intensity focused ultrasound lesions. Ultrasound Med Biol 2006;32:1743–1751.

Smith SW. The scientist and engineer's guide to digital signal processing. San Diego: California Technical Publishing; 1997.

Sokka SD, King R, Hynynen K. MRI-guided gas bubble enhanced ultrasound heating in in vivo rabbit thigh. Phys Med Biol 2003;48: 223–241.

ter Haar GR, Daniels S. Evidence for ultrasonically induced cavitation in vivo. Phys Med Biol 1981;26:1145–1149.

ter Haar GR. Ultrasound focal beam surgery. Ultrasound Med Biol 1995; 21:1089–1100.

Thomas CR, Farny CH, Wu T, Holt RG, Roy RA. Monitoring HIFU lesion formation in vitro via the driving voltage. 5th International Symposium on Therapeutic Ultrasound, Melville, New York 2006:293–297.

Tu J, Matula TJ, Brayman AA, Crum LA. Inertial cavitation dose produced in ex vivo rabbit ear arteries with Optison® by 1-MHz pulsed ultrasound. Ultrasound Med Biol 2006;32:281–288.

Vaezy S, Shi X, Martin RW, Chi E, Nelson PI, Bailey MR, Crum LA. Real-time visualization of high-intensity focused ultrasound treatment using ultrasound imaging. Ultrasound Med Biol 2001;27: 33–42.

Visioli AG, Rivens I, ter Haar GR, Horwich A, Huddart RA, Moskovic E, Padhani A, Glees J. Preliminary results of a phase I dose escalation clinical trial using focused ultrasound in the treatment of localised tumours. Eur J Ultrasound 1999;9:11–18.

Vykhodtseva N, McDannold N, Hynynen K. Progress and problems in the application of focused ultrasound for blood–brain barrier disruption. Ultrasonics 2008;48:279–296.

Watkin NA, ter Haar GR, Rivens I. The intensity dependence of the site of maximal energy deposition in focused ultrasound surgery. Ultrasound Med Biol 1996;22:483–491.

Zeqiri B, Ge PN, Hodnett M, Lee ND. A novel sensor for monitoringacoustic cavitation. Part I. Concept, theory and prototype development IEEE. Trans Ultrason Ferroelectr Freq Control 2003;50:1342–1350.

ADDENDUM

Since the submission of this paper in 2008, the following papers have been published on this topic:

Khokhlova et al. (2009) studied a (transparent) gel phantom using direct visualisation, monitoring of drive power and passive cavitation prior to performing the same exposures in the bore of an MR scanner to distinguish between for boiling and acoustic cavitation activity. (see reference list)

Canney et al. (2010) reported the use of a similar suite of detection techniques (direct imaging, drive voltage, and PCD, but excluding MRI) in a study of micro-second boiling in both gel phantoms and ex-vivo liver tissue. (see reference list)